Fuel 119 (2014) 47–56

Contents lists available at ScienceDirect

Fuel

journal homepage: www.elsevier.com/locate/fuel

High resolution FT-ICR mass spectral analysis of bio-oil and residual water soluble organics produced by hydrothermal liquefaction of the marine microalga *Nannochloropsis salina*

Nilusha Sudasinghe [a], Barry Dungan [a], Peter Lammers [b], Karl Albrecht [c], Doug Elliott [c], Rich Hallen [c], Tanner Schaub [a,*]

[a] Chemical Analysis and Instrumentation Laboratory, New Mexico State University, College of Agricultural, Consumer and Environmental Sciences, 945 College Ave., Las Cruces, NM 88003, USA
[b] Energy Research Laboratory, New Mexico State University, P.O. Box 30001, MSC 3RES Las Cruces, NM 88003, USA
[c] Chemical and Biological Process Development Group, Pacific Northwest National Laboratory, P.O. Box 999, Richland, WA 99352, USA

HIGHLIGHTS

- Detailed analysis of bio-oil produced by hydrothermal liquefaction of marine micro algae.
- Detailed analysis of aqueous phase byproduct from hydrothermal liquefaction of marine micro algae.
- First application of FT-ICR MS to algal HTL bio-oils.
- ID of high MW nitrogen compounds and their distribution in HTL oil and aqueous phase byproduct.

ARTICLE INFO

Article history:
Received 23 August 2013
Received in revised form 30 October 2013
Accepted 10 November 2013
Available online 24 November 2013

Keywords:
Microalgae
Biofuel
Nannochloropsis
Hydrothermal liquefaction
FT-ICR MS

ABSTRACT

We report a detailed compositional characterization of a bio-crude oil and aqueous by-product from hydrothermal liquefaction of *Nannochloropsis salina* by direct infusion Fourier Transform Ion Cyclotron Resonance Mass Spectrometry (FT-ICR MS) in both positive- and negative-ionization modes. The FT-ICR MS instrumentation approach facilitates direct assignment of elemental composition to >7000 resolved mass spectral peaks and three-dimensional mass spectral images for individual heteroatom classes highlight compositional diversity of the two samples and provide a baseline description of these materials. Aromatic nitrogen compounds and free fatty acids are predominant species observed in both the bio-oil and aqueous fraction. Residual organic compounds present in the aqueous fraction show distributions that are slightly lower in both molecular ring and/or double bond value and carbon number relative to those found in the bio-oil, albeit with a high degree of commonality between the two compositions.

1. Introduction

Among current candidate biofuel feedstock, marine microalgae attract attention because their production requires neither arable land nor fresh water [1,2]. Microalgae have a high photosynthetic efficiency which results in fast growth rates and high area-specific yields compared to terrestrial lignocellulosic biomass [3,4]. Because microalgae can utilize nitrogen and phosphorus nutrients from aqueous waste streams and remove heavy metals (e.g. As, Cd and Cr) from wastewater [5], the possibility of microalgal production coupled with waste water treatment programs also appears viable [6]. The marine microalga *Nannochloropsis sp.* in particular have shown potential as a bio-diesel feedstock due to high lipid content and growth rate [7–9]. Rodolfi et al. [10] screened thirty microalgal strains for lipid production potential and reported three members of *Nannochloropsis sp.* exhibited the best combination of biomass productivity and lipid content. *Nannochloropsis salina* has received considerable attention as a biofuel production candidate with scalable production of *N. salina* (CCMP 1776) biomass in closed photobioreactors over a 2.5 year period showing an average lipid production of 10.7 $m^3\ ha^{-1}\ yr^{-1}$ and a peak value of 36.3 $m^3\ ha^{-1}\ yr^{-1}$ [11].

Lipid-only based biodiesel production utilizes only a portion of available algal biomass and cultivation strategies that employ stress-induced lipid accumulation often result in diminished biomass productivity. Therefore, thermochemical fuel production schema that utilize whole algal biomass are of interest and process

* Corresponding author. Tel.: +1 575 646 5156; fax: +1 575 646 1597.
E-mail address: tschaub@nmsu.edu (T. Schaub).

0016-2361/$ - see front matter © 2013 Published by Elsevier Ltd.
http://dx.doi.org/10.1016/j.fuel.2013.11.019

optimization for these routes is underway [6,12]. Thermochemical conversion processes for microalgal biofuel production include pyrolysis [13,14] and gasification [15,16] both of which convert dry biomass to bio-oil. However, due to the high mass percentage of water in microalgal growth medium (>99%) and the associated energy expense of concentration, dewatering and drying, these conventional thermochemical processes are not feasible at scale. Wet processes like hydrothermal liquefaction (HTL) and hydrothermal gasification appear more suitable for biofuel production from microalgae feedstock [12]. During hydrothermal liquefaction, wet biomass is subjected to elevated temperature (280–370 °C) and pressure (10–25 MPa) in the presence of water to decompose and reform biomass into a bio-oil, aqueous fraction, gases and solid by-products [3].

Fourier transform ion cyclotron resonance mass spectrometry (FT-ICR MS) has been widely used for the compositional description of petroleum crude oils owing to ultra-high mass resolving power (i.e. $m/\Delta m_{50\%} = 400{,}000$ at m/z 400, where $\Delta m_{50\%}$ is the mass spectral peak width at half-maximum peak height) and sub part-per-million mass measurement accuracy, both of which are required for analysis of mixtures of that complexity [17,18]. For example, FT-ICR MS has been used to successfully observe tens of thousands of compounds simultaneously in petroleum crude oil [19–24]. In addition, bio-oils derived from fast pyrolysis of various biomass feedstock have also been characterized by this technique [25,26] and we have recently used this approach to describe the composition of complex algal lipid extracts as well [27]. Here, we apply that approach to the characterization of bio-crude oil and water soluble organics derived from hydrothermal liquefaction of *N. salina* by both positive- and negative-ion electrospray ionization FT-ICR MS to provide a baseline description of the composition of these materials. These data illustrate heteroatom and functionality distribution to provide a means for process optimization and selection of appropriate upgrading strategy.

2. Materials and methods

2.1. Production of HTL bio-oil

N. salina biomass was provided by Solix Biosystems. After harvest, the sample was centrifuged to ~20–25% solids and frozen immediately. Gravimetrically-determined lipid content of the whole algae was 33 wt% (ash-free dry weight, AFDW) for a Folch extraction [28]. Table 1 shows results of elemental analysis and ash determinations of the whole-algae feedstock and the resulting HTL bio-oil.

For bio-oil production, a continuous-feed reactor system was used (Fig. 1) that consists of a high-pressure pump feeding system, preheater, oil jacketed (stirred tank) and plugged-flow reactor stages, solids separator and product liquid collectors. The solids separator is primarily for mineral separation (very little char material is produced with algal feedstock). The bio-oil and aqueous products are recovered in alternating 1-L high-pressure vessels. The system size was operated at a throughput of 1.5 L of algal slurry per hour and over a test period of 10 h.

The pumping subsystem consists of a modified Isco 500D pump (Teledyne, Lincoln, NE). Slurry feed rate is measured directly from the screw drive of the positive displacement syringe pump and algal slurry is pumped without additional preparation. Incoming slurry is heated in an oil-heated jacketed tube in shell heat exchanger prior to being heated to a reaction temperature of 350 °C in a 1-L stirred tank reactor that is equipped with internal stirring propellers. System pressure was 20.3 MPa. The reactor function as a continuous-flow, stirred-tank reactor and additional reaction time is provided by a heated plug-flow portion of process tubing thereafter. This reactor configuration is based on experiences processing lignocellulosic feedstock. As part of the liquefaction process, inorganic components such as calcium phosphate precipitated as solids. A separator vessel was placed in the process line following the reactor to capture and remove the solids near the reaction temperature (~345 °C). The design of the separator was a simple dip leg vessel where solids fell to the bottom of a vessel and liquid passed overhead through a filter to the reactor. The solids could be removed by batch from the bottom of the vessel and this in-line system provides a solids-free bio-oil product that readily separates from the water fraction.

After exiting the solids separator, the products were conducted to a two-tank liquid collecting system where condensed liquids are collected at pressure. Here, system flow is periodically directed from the first to the second collection vessel and in this way the liquid product collection vessels are alternately filled and drained. Gas byproducts were vented overhead through a back-pressure regulator to the process vent where it was metered and sampled for offline gas chromatographic analysis (primarily CO_2 and water vapor). Liquid product was drained from the collectors into sample holding jars where a lighter oil and heavier aqueous fraction form spontaneously and are readily separated by cooling the sample and pouring the water from the oil.

Table 1
Elemental analysis and ash content for *N. salina* HTL feedstock and produced bio-oil.

Source	C (%)	H (%)	O (%)	N (%)	S (%)	Ash (%)
Whole algae	55.9	8.3	23.7	4.1	0.6	7.4
HTL bio-oil	77.9	10.2	5	4.6	0.42	0.1

2.2. Sample preparation and FT-ICR mass spectrometry

An HTL bio-oil stock mixture was prepared by dissolving the oil in 1:1 chloroform: methanol to a concentration of 1 mg/mL. For positive ion mode mass spectral analysis, the stock mixture was further diluted to 0.5 mg/mL in an electrospray ionization solution of 1:2:4 chloroform:methanol:2-propanol containing 0.1% formic acid as an electrospray ionization modifier (for observation of basic compounds). For negative ion mode analysis, the initial oil stock mixture was further diluted to 0.1 mg/mL with 1:2:4 chloroform:methanol:2-propanol containing 0.1% ammonium hydroxide (for observation of acidic compounds). Addition of modifiers to the spray solution facilitates protonation or deprotonation in each ionization mode.

For the analysis of water soluble organics, the aqueous fraction was diluted 200-fold and 1000-fold in positive- and negative-ion modes, respectively in the electrospray ionization solutions listed above. All solvents were HPLC grade and purchased from Sigma–Aldrich (St. Louis, MO). Final prepared solutions were filtered through Acrodisc CR 13 mm syringe filters with 0.2 μm PTFE membranes (Pall Corporation, Ann Arbor, MI) prior to FT ICR-MS analysis to remove any suspended particulate materials.

High-resolution FT-ICR mass spectrometry was performed with a hybrid linear ion trap FT-ICR mass spectrometer (LTQ FT, Thermo Fisher, San Jose, CA) equipped with a 7 Tesla superconducting magnet. Mass resolving power was $m/\Delta m_{50\%} = 400{,}000$ at m/z 400 (time-domain transient length was 3 s). Direct infusion of the samples was performed with an Advion Triversa Nanomate (Advion, Ithaca, NY). A total of 450 and 350 time-domain transients were ensemble averaged for each sample in positive and negative ion modes, respectively prior to fast Fourier transformation and frequency to mass-to-charge ratio conversion.

Mass spectra were internally mass calibrated to provide sub-part-per-million mass measurement accuracy which facilitates direct assignment of elemental composition from measured m/z

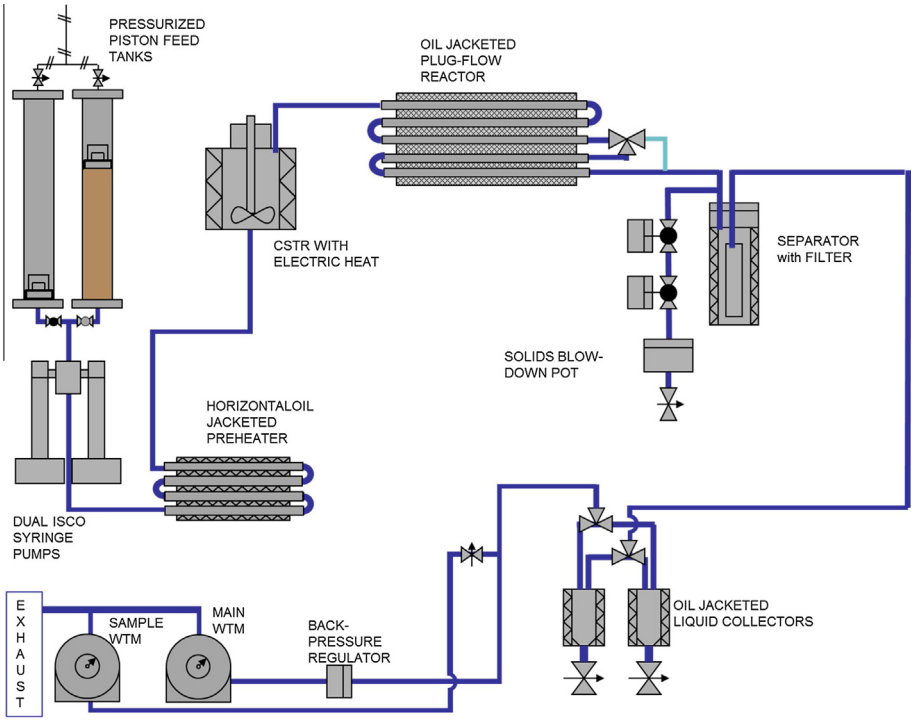

Fig. 1. Process flow configuration for microalgal hydrothermal liquefaction.

value. This procedure utilizes signals from a homologous series of known compounds (i.e. species that differ in elemental composition by multiples of CH_2) to perform frequency to *m*/*z* conversion. Peak lists were generated to include signals observed at S/N > 6. Elemental compositions assigned for ~95% of all observed peaks for both HTL bio-oil and aqueous fraction in the positive ion mode and ~75% of all observed peaks for negative ion mode spectra. The mass measurement accuracy for all assigned elemental compositions is 0.260 ppm_{rms} and 0.187 ppm_{rms} for the HTL bio-oil and the aqueous fraction, respectively.

Tandem mass spectrometry (collision induced dissociation, CID) was performed for several major species observed in abundant heteroatom classes and for abundant Kendrick series thereof to correlate elemental compositions with possible molecular structures where possible. Ions of interest were isolated and fragmented to obtain MS^2 and MS^3 spectra, however isolation of some peaks from the broadband mass spectra was impossible due to the high complexity of the samples and limited selection specificity of the linear ion trap CID process. Compounds were identified from MS^n spectra by manual inspection and matching to reference spectra where possible.

3. Results and discussion

The hydrothermal liquefaction process converted 64% (AFDW) of the algal biomass to organic fraction bio-oil and 69% of the carbon present in the algae feedstock was incorporated in the bio-oil. Broadband ESI FT-ICR mass spectra (two ionization modes) for HTL bio-oil and the reaction aqueous fraction are shown in Fig. 2. The observed mass spectral complexity requires FT-ICR mass spectrometry to resolve several thousand ion signals per mass spectrum. The positive-ion ESI FT-ICR mass spectrum of HTL bio-oil is more compositionally complex than the aqueous fraction (~4600 versus ~3370 mass spectral peaks). However, the opposite trend was observed for negative-ion ESI FT-ICR spectra where the aqueous fraction shows higher complexity than the HTL bio-oil (~2770 versus ~1740 peaks, respectively). The observed mass-average molecular masses are 431 and 319 Da, for positive ion and negative ion mode, respectively. Interestingly, we observe minimal contribution from small molecules (i.e. less than *m*/*z* ~150) and have verified that observation through electrospray ionization analyses with a linear ion trap mass spectrometer, for which ion transmission is appreciably less mass-selective than our FT-ICR system (especially at low *m*/*z*). Signal magnitudes obtained are proportional to solution phase concentration for infusion solutions but response factors for each compound are unknown. Therefore the comparative analysis shown here represents a detailed qualitative, rather than quantitative, description of these materials.

As reported for similar analyses of petroleum, assigned elemental compositions are sorted based on heteroatom content, molecular rings/and or double bonds (double bond equivalents, DBE) and carbon number. In particular, three-dimensional mass spectral images of DBE versus the carbon number (with relative abundance expressed as color) are useful to visualize broad trends and compositional variation in terms of degree of alkylation (carbon number) and aromaticity (DBE). These analyses simplify the complex nature of the data and facilitate comparative analysis between samples. The distribution of heteroatoms is shown for both the HTL bio-oil and the aqueous fraction for negative ion (Fig. 3, top) and positive ion mode class analyses (Fig. 3, bottom). For simplicity, only compound classes that comprise 95% of the total ion abundance are shown. Although both ^{32}S and ^{31}P were considered in the elemental composition assignment process, heteroatom classes containing sulfur or phosphorous exhibit less than 0.4% relative abundance in either sample.

3.1. Negative ions (acidic species)

The heteroatom class distribution for HTL bio-oil and aqueous fraction negative-ion ESI FT-ICR MS (Fig. 3) show that acidic compounds in the bio-oil are primarily comprised of O_2 species.

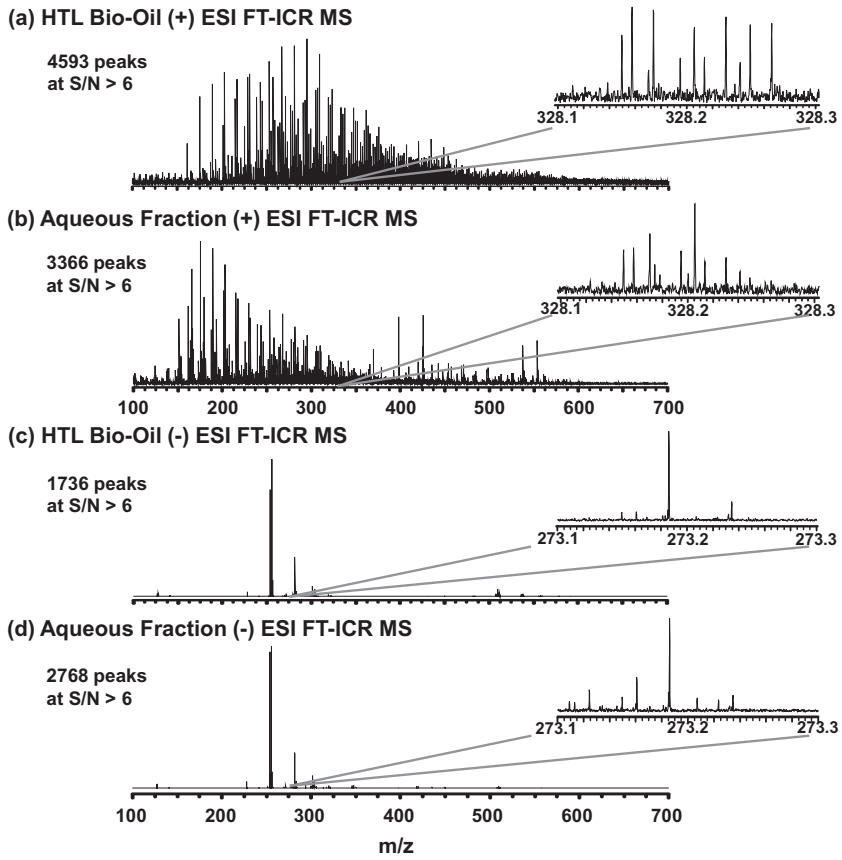

Fig. 2. Broadband ESI FT-ICR mass spectra of *N. salina* hydrothermal liquefaction products (a) positive-ion mode mass spectrum of HTL bio-oil (b) positive-ion mode mass spectrum of aqueous fraction (c) negative-ion mode mass spectrum of HTL bio-oil (d) negative-ion mode mass spectrum of aqueous fraction.

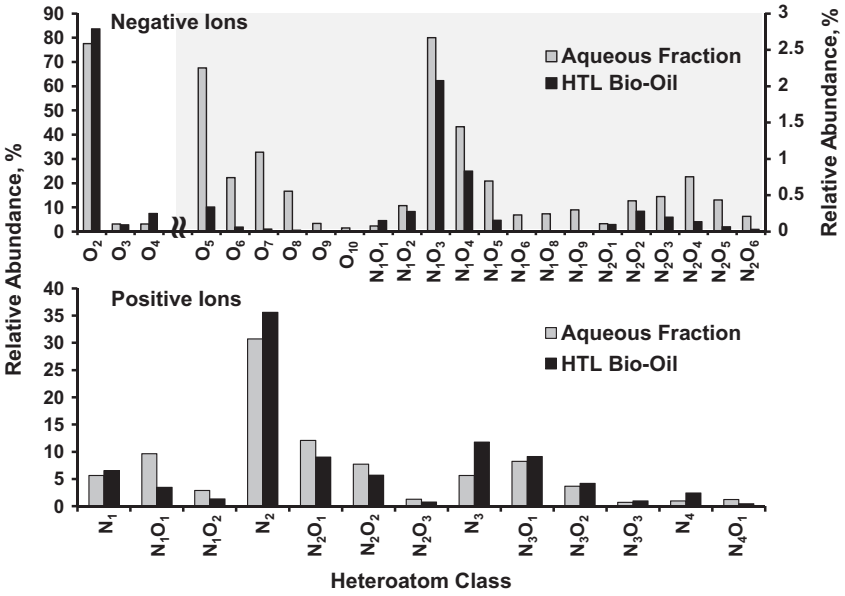

Fig. 3. Heteroatom class distribution for hydrothermal liquefaction oil and aqueous fraction derived from negative ion mode (top) and positive ion mode (bottom) ESI FT-ICR mass spectra. Only classes that comprise 95% of the total ion abundance are shown.

The aqueous fraction contains a more diverse distribution of acidic compound classes including oxygenates with up to 10 oxygen atoms and $N_{1-2}O_x$ species, with O_2 being the most abundant class observed. This broad range of oxygenated compounds can arise from the decomposition of cellulose or other carbohydrates during the HTL process [29]. As reported for petroleum, oxygenated functional groups increase water solubility for acidic nitrogen species [30]. The negative-ion FT-ICR MS class distribution demonstrates that non-basic nitrogen-containing compounds are soluble in water only if they contain an oxygenated functional group. The

presence of oxygenated functional groups enhance the water solubility of nitrogen heterocyclics with higher DBE and higher carbon number (e.g. carbazole) which are otherwise only slightly soluble in water due to their high aromaticity [29,31]. Previous work has demonstrated that basic nitrogen containing compounds (e.g. pyridinic compounds) are selectively ionized by positive-ion ESI, [24,32] whereas acidic nitrogen containing compounds (e.g. pyrrolic compounds) are selectively ionized by negative-ion ESI [22,33]. Similarly, the distributions of observed N_1O_x species observed here are likely pyrrole, indole and carbazole derivatives with oxygenated functional groups.

3.1.1. O_2 compounds

The abundance-contoured three dimensional mass spectral images constructed for acidic O_2 compounds for HTL bio-oil and aqueous fraction show similar distribution of compounds in terms of DBE and carbon number (data not shown). Both samples show primarily O_2 species with carbon numbers of 14–20 and DBE values of 0–3, which correspond directly to the distribution of free-fatty acids expected from the known acyl-hydrocarbon distribution for this species [6,34]. Tandem mass spectrometry confirms the identification of abundant O_2 compounds as free fatty acids, dominated by palmitic and palmitoleic acid. These long chain free fatty acids may exist in the aqueous fraction as micro-emulsions due to their hydrophobic character [26]. Some O_2 compounds with higher DBE (i.e. DBE = 5,6) were also observed for both samples and among those compounds, high relative abundances were observed for eicosapentaenoic acid (EPA) (~1.2% and ~0.6% relative abundance for HTL bio-oil and aqueous fraction, respectively) and arachidonic acid (~0.8% and ~0.4% total relative abundance for HTL bio-oil and aqueous fraction, respectively). In addition, several O_2 species with lower carbon number (C_7–C_{13}) and higher DBE (DBE 5) were detected only in the aqueous fraction. Those compounds were identified as aromatic carboxylic acids by tandem mass spectrometry.

3.1.2. O_4 compounds

Predominant O_4 class compounds detected in the negative-ion ESI FT-ICR MS correspond to di-carboxylic acids formed as a result of polymerization of fatty acids (Fig. A.1, supplementary material). Not surprisingly, the most abundant O_4 compound in HTL bio-oil is DBE = 2 and contains 32 carbon atoms. These long chain di-acids were also observed in the aqueous fraction, but with very low abundance. In addition, several abundant saturated di-carboxylic acids with low carbon number (C_4–C_{12}) were observed in the aqueous fraction (confirmed by MS/MS experiments) and were not detected in the HTL bio-oil. Linear ion trap MS/MS fragment ion spectra for di-carboxylic acids with carbon number = 4 and 5 observed in the aqueous fraction are shown in Fig. A.2 (supplementary material) [53,54].

3.2. Positive ions (basic species)

The predominant compound classes observed in positive ion mode for both samples are basic nitrogen compounds with 0–3 oxygen atoms (Fig. 3, bottom). The most abundant class observed in both the HTL bio-oil and aqueous fraction contains two nitrogen atoms per molecule and no oxygen atoms. Generally, for a given number of nitrogen atoms, abundance decreases with an increase of oxygen number.

3.2.1. Basic N_1 compounds

Degradation of amino acids during the HTL process can produce a variety of N_1 compounds. For example, decarboxylation, dehydrogenation, dehydration and loss of ammonia can result various alkyl and aromatic amines, nitriles and imines whose structures depend on the nature of the amino acid [35]. Abundance-contoured plots of DBE versus carbon number for basic N_1 compounds observed in both samples are shown in Fig. 4. The primary N_1 compounds in HTL bio-oil have double bond equivalent values of 4–13 and contain 12–27 carbon atoms. However, we do not observe a broad distribution of DBE and carbon number for major N_1 compounds observed in the aqueous fraction. The regions of highest abundance for aqueous fraction show a shift to lower carbon number compared to those in the HTL bio-oil although they exhibit the same DBE (for example DBE = 6 and DBE = 9). For further clarification, carbon number distribution plots for the "hotspots" at DBE = 6 and DBE = 9 for both samples are shown in Fig. 5.

Observed N_1, DBE = 4 compounds in both HTL bio-oil and the aqueous fraction are pyridine derivatives (Fig. A.3, supplementary material), with positive-ion electrospray selectively ionizing these basic nitrogen-containing compounds [32]. Ionization of basic pyridine homologues by positive-ion ESI is expected because the lone-pair of electrons on the nitrogen atom in pyridine are available for protonation in the electrospray ionization process. The DBE = 5 "hotspot" observed for the aqueous fraction and less-so in the HTL bio-oil (Fig. 4) would indicate alkyl-substituted pyridine compounds with an additional double bond in the alkyl chain. The high abundance compounds at DBE = 6 correspond to pyridine derivatives with two double bonds contained in alkyl positions and similarly-abundant DBE = 9 compounds correspond to quinoline derivatives with two double bonds in alkyl positions. These compounds exhibit low solubility in the aqueous fraction due to increased hydrophobicity of high carbon number compounds. Low carbon number (C < 15) N_1 compounds with 0–3 DBE observed in the aqueous fraction are amines and no compounds with <4 DBE are observed in the HTL bio-oil.

3.2.2. Basic N_2 compounds

The number of molecular rings and/or double bonds for N_2 compounds for both HTL bio-oil and the aqueous fraction range from one to twenty-one (Fig. A.4, supplementary material). For the aqueous fraction, relative abundance maxima occur at three regions; DBE = 4, 6 and 9. N_2 species with DBE = 3 and 4 observed in both HTL bio-oil and aqueous fraction are likely imidazole (DBE = 3) and pyrazine (DBE = 4) derivatives with latter being more abundant in both samples.

Fig. 6 shows abundance-contoured plots of DBE versus carbon number for the N_2 class. Major N_2 compounds observed in the HTL bio-oil show DBE = 4–15 and carbon content of 9–28 atoms. Again the aqueous fraction shows a marked shift to lower DBE and lower carbon number (primary compounds with DBE = 2–11 and 8–20 carbon atoms). This shift derives from improved water solubility of N_2 compounds by decreased DBE (aromaticity) and decreased carbon number (alkylation) [36]. For the HTL bio-oil, relative abundance maxima are observed at DBE = 6, 7, 9 and 10. The aqueous fraction shows the highest relative abundance at DBE = 6, carbon number of 11–12. Also we observe two less abundant compositional regions of high abundance for the aqueous fraction at DBE = 4, carbon number = 10 and DBE = 9, carbon number = 17–18.

The carbon number distribution for N_2 class DBE = 6 compounds and that for N_2 DBE = 9 compounds is shown in Fig. A.5, supplementary material. The DBE = 6 and 9 species observed in both HTL bio-oil and the aqueous fraction (Fig. 6) are two- and three-ring imidazole derivatives formed by the successive addition of aromatic rings to the imidazole core (DBE = 3). The DBE = 9 compounds show low abundance in the aqueous fraction compared to the compounds with 6 DBE due to their increased aromaticity. Linear ion trap MS/MS fragmentation with FT-ICR MS detection (Fig. A.6, supplementary material) confirms that N_2 compound correspond to the "hotspot" at DBE = 6, carbon number = 11 for the aqueous fraction is alkylated benzimidazole derivative. These

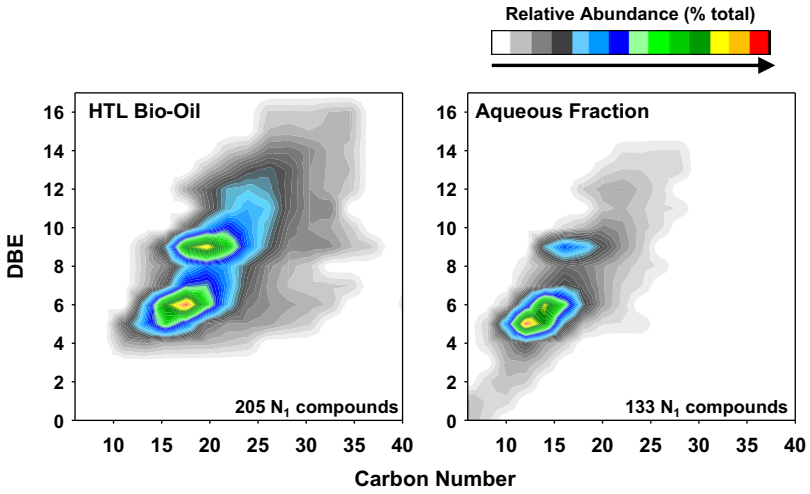

Fig. 4. Color-coded isoabundance-contoured plots of DBE versus carbon number for N_1 compounds for HTL bio-oil (left) and aqueous fraction (right) derived from positive-ion ESI FT-ICR mass spectra.

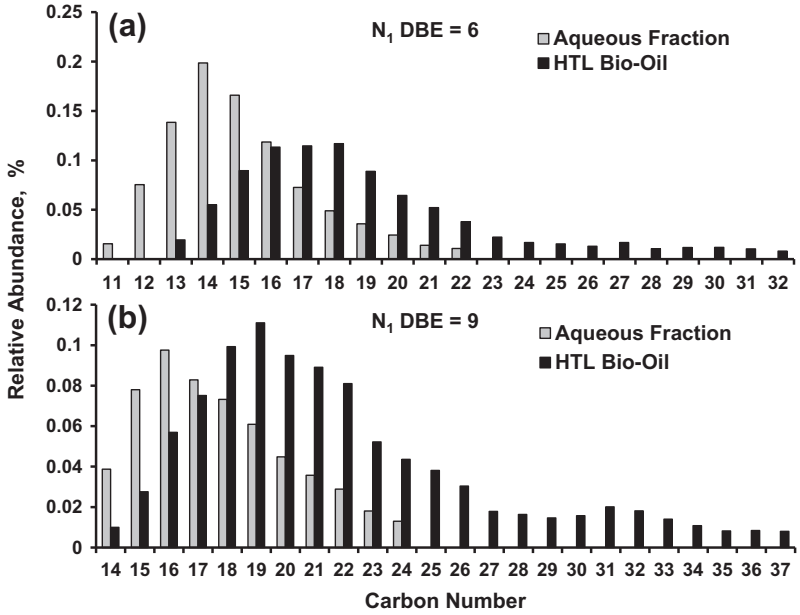

Fig. 5. Carbon number distribution for (a) DBE = 6 and (b) DBE = 9 compounds observed in the N_1 class for HTL bio-oil and aqueous fraction from (+) ESI FT-ICR MS.

imidazole compounds are assumed to be present in the sample as a result of protein decomposition [29]. Bio-oil DBE = 7 and 10 species are indicative of quinoxaline (benzopyrazine) and phenazine (dibenzopyrazine) which can result by the addition of 1 and 2 benzene rings, respectively to pyrazine (DBE = 4). These pyrazine compounds are formed by the decomposition of Melanoidin-like polymers formed during the Maillard reaction between amino acids and reducing sugars [37].

3.2.3. N_3 compounds

Three-dimensional mass spectral images of N_3 compounds observed in the HTL bio-oil and aqueous fraction in the positive ion mode are shown in Fig. 7. HTL bio-oil contains more N_3 compounds than the aqueous fraction (288 versus. 181 individual N_3 compounds). The highest relative abundances were observed at DBE = 10, carbon number = 25–30 and DBE = 9, carbon number = 15–20 for the HTL bio-oil and the aqueous fraction, respectively. To compare the DBE and the carbon number distribution of N_3 compounds in the HTL bio-oil and the aqueous fraction, we have highlighted the predominant compounds observed in the aqueous fraction and overlaid the oval on that for the HTL bio-oil. The aqueous fraction is enriched with low carbon number (low molecular weight) and low DBE compounds compared to the HTL bio-oil. Major N_3 compounds in the aqueous fraction range from DBE = 6–17 and carbon number C = 10–30, whereas primary species in the HTL bio-oil span the range DBE = 8–18 and C = 17–38. Tandem mass measurement was not possible for these compounds because they cannot be isolated from nearby nominal mass isobars for selection/fragmentation. The proposed molecular structures for the observed N_3 compounds are alkyl-substituted pyridyl-piperazines, alkylated amine substituted pyridines and imidazoles.

3.2.4. N_xO_y compounds

Abundance-contoured mass spectral images for N_1O_1, N_2O_1, N_2O_2 and N_3O_1 compounds observed in both HTL bio-oil and the

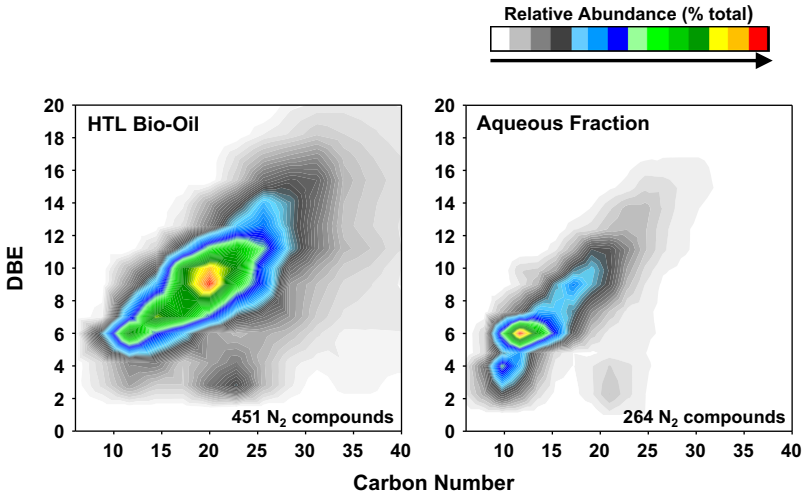

Fig. 6. Color-coded abundance-contoured plots of DBE versus the carbon number for N_2 compounds for HTL bio-oil (left) and aqueous fraction (right) derived from positive-ion ESI FT-ICR MS.

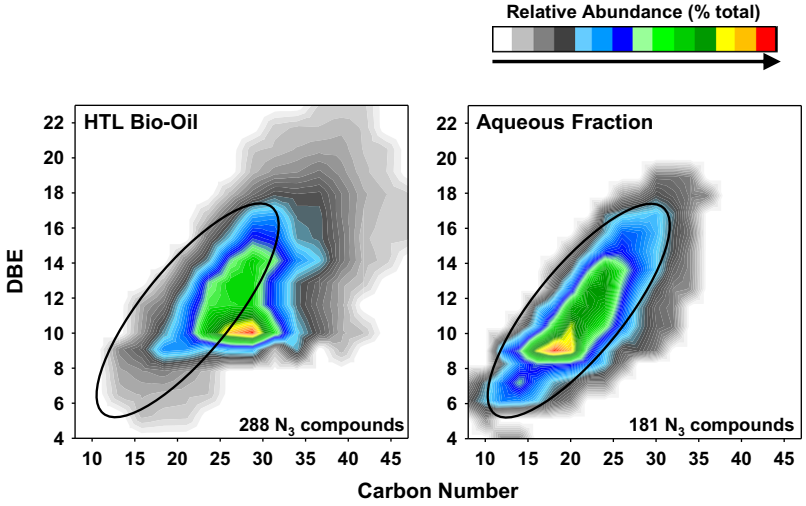

Fig. 7. Color-coded abundance-contoured plots of DBE versus the carbon number for N_3 compounds for HTL bio-oil (left) and aqueous fraction (right) derived from positive-ion ESI FT-ICR MS.

aqueous fraction are shown in Fig. 8. Similar to the classes discussed above (i.e. N_1, N_2 and N_3), high carbon number and high DBE compounds are predominant in the HTL bio-oil, whereas aqueous fraction exhibit relatively low carbon number and low DBE species. The N_1O_1 compounds with 0–4 DBE and 14–24 carbons observed in both samples are likely fatty-amides formed by the reaction between fatty acids and ammonia (from protein decomposition) at high temperature [38]. N_1O_1 species observed in the HTL bio-oil which span the range, DBE = 3–16 and carbon number C = 8–30 are aromatic amides that exhibit poor solubility in the aqueous fraction due to their high aromaticity and high carbon number.

Observed N_2O_1 and N_2O_2 compounds are likely oxygenated alkyl-imidazoles and oxygenated alkyl-pyrazines (tandem mass spectrometry confirmation was not available for these ions). The abundance-contoured mass spectral images demonstrate similar carbon number distributions (C_{6-35}) for N_2, N_2O_1 and N_2O_2 compounds observed in the aqueous fraction. The predominant N_2O_1 and N_2O_2 compounds exhibit increased DBE and increased carbon number compared to the N_2 species; highlighting that incorporation of oxygenated functional groups into N_2 compounds enhances the water solubility of higher carbon number compounds. In addition, N_2O_2 compounds may include cyclic dipeptides such as diketopiperazines (DKP) formed by degradation of peptides through depolymerization and cyclization [35]. Note that for N_2O_2 species, dipeptides with amino acids containing alkyl side chains should only be considered. These DKPs can extend from 6 to 18 carbons and 2–10 DBE depending on the structure of the two amino acids.

N_3O_1 compounds observed are probably oxygenated versions of the N_3 compounds discussed earlier. Carbon number distributions of N_3 and N_3O_1 compounds for each sample confirm that both N_3 and N_3O_1 species contain the same number of carbon atoms per molecule. Interestingly, the "hotspot" at DBE = 10, carbon number C = 25–30 for the N_3 compounds in the HTL bio-oil is observed for the N_3O_1 compounds at the same carbon number but with shifted DBE by +1 DBE, suggesting that the oxygen atom is likely attached to the molecule as carbonyl oxygen.

Oxygenated functional groups improve the water solubility of nitrogen compounds with low DBE and high carbon number. For example, note the presence of N_2O_1 and N_3O_1 compounds with 0–2 DBE and ~20–40 carbons in the aqueous fraction with high abundance, which are less abundant or absent in the HTL bio-oil.

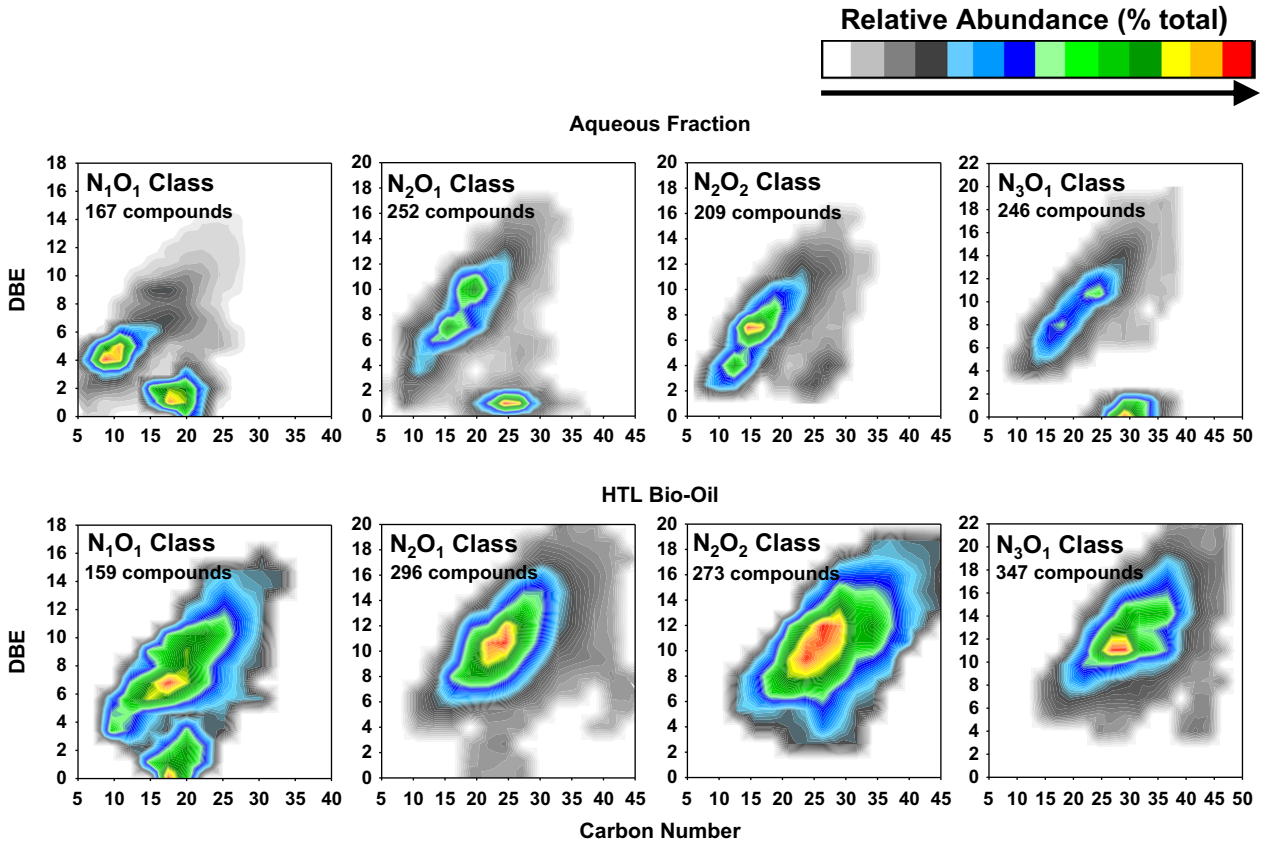

Fig. 8. Color-coded abundance-contoured plots of DBE versus the carbon number for N_1O_1, N_2O_1, N_2O_2 and N_3O_1 classes for aqueous fraction (top) and HTL bio-oil (bottom) derived from positive-ion ESI FT-ICR MS.

4. Conclusion

The detailed compositional analysis shown here for bio-oil and the aqueous HTL fraction of *N. salina* provides baseline description for several thousand chemically unique compounds present in these two HTL products. We observe a range of heteroatom-containing chemical compounds including oxygenated species and various nitrogenous compounds with extensive carbon number distributions in both samples. Oxygenated compounds are likely formed by the degradation of lipids and carbohydrates whereas protein decomposition (and cross reaction of other products) yield numerous nitrogen heterocyclics (e.g. pyrroles, pyridines, pyrazines, imidazoles and their derivatives).

Thorough compositional analysis of HTL bio-oil is essential for feedstock selection and process optimization. The commonly used analytical methods for the characterization of bio-oil include gas chromatography/flame ionization detection (GC-FID) [6] and gas chromatography coupled with mass spectrometry (GC–MS) [39–41]. Chromatography techniques lack both the resolution and selectivity for direct speciation of these mixtures, particularly with respect to nitrogen-containing compounds characteristic of bio-crude oil. Highly oxygenated species present in the bio-oil are also not well-addressed by chromatographic techniques due to their high polarity [26]. In addition, GC–MS is not capable of detecting high molecular mass species which are present in these oils [42]. Several techniques that have been reported for characterization of the fractions of bio-oil not detectable by GC include Fourier transform infrared spectroscopy (FTIR) [39,43], high pressure liquid chromatography [41], ^{1}H NMR[44], ^{13}C NMR [45] and size exclusion chromatography [41] and gel permeation chromatography [46]. These techniques supply bulk compositional information that serves for partial characterization of these materials but lack sufficient resolution to describe individual components present in highly complex bio-crude oil. The ability to track the response of individual constituent molecules is particularly useful for HTL process optimization and for monitoring upgrading process efficiency.

The potential use of algal hydrothermal liquefaction bio-oil as feedstock for production of transportation fuel will require removal of these polar species to limit corrosion, [47] fuel instability during storage and emission of NO_x compounds upon combustion, [48] for example. Among available upgrading methods, hydrotreatment appears a probable technique for treatment of these materials [49,50] and optimization of that process is currently underway. As reported for petroleum crude oil, N_1 compounds are more hydrotreatment-resistant than compounds with additional nitrogen or oxygen heteroatoms [51]. Within the N_1 class, nitrogen containing compounds with unsaturated core structures and reduced alkyl substitution (and length) are more readily removed by hydrotreating than those compounds which contain long alkyl moieties [52]. Basic nitrogen compounds (e.g. pyridine derivatives) have a higher conversion rate than the acidic or neutral nitrogen species (e.g. pyrrole and indole compounds) [49]. Zhang et al. [52] constructed a criterion to predict the reactivity of the N_1 compounds during the hydrotreatment process by defining an easy-to-convert region in terms of DBE and carbon number. The compounds that fall within this region are reactive and thereby easily removed by hydrotreatment. The N_1 compounds observed in the HTL bio-oil in our study extend to DBE = 17 and 37 carbon atoms per molecule. A considerable fraction of these observed N_1 compounds fall within

Zhang's "easy-to-convert" region, and should be readily converted by hydrotreatment.

In summary, we demonstrate FT-ICR MS an effective technique for detailed compositional characterization (at the molecular level) of complex HTL products and by-products. We illustrate HTL bio-oil composition for improved understanding of bio-crude and further improvement in the HTL bio-oil production and upgrading processes.

Acknowledgements

We thank Omar Holguin for helpful discussions. This work was supported by the U.S. Department of Energy under contract DE-EE0003046 awarded to the National Alliance for Advanced Biofuels and Bioproducts, the National Science Foundation (IIA-1301346) and the Center for Animal Health and Food Safety at New Mexico State University.

Appendix A. Supplementary material

Supplementary material associated with this article can be found, in the online version, at http://dx.doi.org/10.1016/j.fuel.2013.11.019.

References

[1] Campbell MN. Biodiesel: algae as a renewable source for liquid fuel. Guelph Eng J 2008;1:2.
[2] Patil V, Tran KQ, Giselrod HR. Towards sustainable production of biofuels from microalgae. Int J Mol Sci 2008;9:1188.
[3] Barreiro DL, Prins W, Ronsse F, Brilman W. Hydrothermal liquefaction (HTL) of microalgae for biofuel production: state of the art review and future prospects. Biomass Bioenergy 2013;53:113.
[4] Posten C, Schaub G. Microalgae and terrestrial biomass as source for fuels – a process view. J Biotechnol 2009;142:64.
[5] Sawayama S, Inoue S, Dote Y, Yokoyama S-Y. CO_2 fixation and oil production through microalga. Energy Convers Manage. 1995;36:729.
[6] Brown TM, Duan P, Savage PE. Hydrothermal liquefaction and gasification of *Nannochloropsis sp*. Energy Fuels 2010;24:3639.
[7] Gouveia L, Oliveira AC. Microalgae as a raw material for biofuels production. J Ind Microbiol Biotechnol 2009;36:269.
[8] Chisti Y. Biodiesel from microalgae. Biotechnol Adv 2007;25:294.
[9] Griffiths MJ, Harrison STL. Lipid productivity as a key characteristic for choosing algal species for biodiesel production. J Appl Phycol 2009;21:493.
[10] Rodolfi L, Chini Zittelli G, Bassi N, Padovani G, Biondi N, Bonini G, et al. Microalgae for oil: strain selection, induction of lipid synthesis and outdoor mass cultivation in a low-cost photobioreactor. Biotechnol Bioeng 2009;102:100.
[11] Quinn JC, Yates T, Douglas N, Weyer K, Butler J, Bradley TH, et al. Nannochloropsis production metrics in a scalable outdoor photobioreactor for commercial applications. Bioresour Technol 2012;117:164.
[12] Elliott CE. Historical developments in hydroprocessing bio-oils. Energy Fuels 2007;21:1792.
[13] McKendry P. Energy production from biomass (part 2): conversion technologies. Bioresour Technol 2002;83:47.
[14] Miao X, Wu Q, Yang C. Fast pyrolysis of microalgae to produce renewable fuels. J Anal Appl Pyrol 2004;71:855.
[15] Amin S. Review on biofuel oil and gas production processes from microalgae. Energy Convers Manag 2009;50:1834.
[16] Tsukahara K, Sawayama S. Liquid fuel production using microalgae. J Jpn Petrol Inst 2005;48:251.
[17] Marshall AG, Hendrickson CL, Jackson GS. Fourier transform ion cyclotron resonance mass spectrometry: a primer. Mass Spectrom Rev 1998;17:1.
[18] Rodgers RP, Schaub TM, Marshall AG. Petroleomics: MS returns to its roots. Anal Chem 2005;77:21 A.
[19] Fernandez-Lima FA, Becker C, McKenna AM, Rodgers RP, Marshall AG, Russell DH. Petroleum crude oil characterization by IMS-MS ans FTICR MS. Anal Chem 2009;81:9941.
[20] Schaub TM, Rodgers RP, Marshall AG, Qian K, Green LA, Olmstead WN. Speciation of aromatic compounds in petroleum refinery streams by continuous flow field desorption ionization FT-ICR mass spectrometry. Energy Fuels 2005;19:1566.
[21] Marshall AG, Rodgers RP. Petroleomics: chemistry of the underworld. Proc Nat Acad Sci USA 2008;105:18090.
[22] Qian K, Robbins WK, Hughey CA, Cooper HJ, Rodgers RP, Marshall AG. Resolution and identification of elemental compositions for more than 3000 crude acids in heavy petroleum by negative-ion microelectrospray high-field Fourier transform ion cyclotron resonance mass spectrometry. Energy Fuels 2001;15:1505.
[23] Stanford LA, Rodgers RP, Marshall AG, Czarnecki J, Wu XA, Taylor S. Detailed elemental compositions of emulsion interfacial material versus parent oil for nine geographically distinct light, medium, and heavy crude oils, detected by negative- and positive-ion electrospray ionization Fourier transform ion cyclotron resonance mass spectrometry. Energy Fuels 2007;21:973.
[24] Qian K, Rodgers RP, Hendrickson CL, Emmett MR, Marshall AG. Reading chemical fine print: resolution and identification of 3000 nitrogen-containing aromatic compounds from a single electrospray ionization Fourier transform ion cyclotron resonance mass spectrum of heavy petroleum crude oil. Energy Fuels 2001;15:492.
[25] Smith EA, Park S, Klein AT, Lee YJ. Bio-oil analysis using negative electrospray ionization: comparative study of high-resolution mass spectrometers and phenolic versus sugaric components. Energy Fuels 2012;26:3796.
[26] Jarvis JM, McKenna AM, Hilten RN, Das KC, Rodgers RP, Marshall AG. Characterization of pine pellet and peanut hull pyrolysis bio-oils by negative-ion electrospray ionization Fourier transform ion cyclotron resonance mass spectrometry. Energy Fuels 2012;26:3810.
[27] Holguin OF, Schaub TM. Characterization of microalgal lipid feedstock by direct-infusion FT-ICR mass spectrometry. Algal Res 2013;2:43.
[28] Folch J, Lees M, Stanley GHS. A simple method for the isolation and purification of total lipids from animal tissues. J Biol Chem 1957;226:497.
[29] Torri C, Garcia Alba L, Samorì C, Fabbri D, Brilman DWF. Hydrothermal Treatment (HTT) of microalgae: detailed molecular characterization of htt oil in view of htt mechanism elucidation. Energy Fuels 2012;26:658.
[30] Stanford LA, Kim S, Klein GC, Smith DF, Rodgers RP, Marshall AG. Identification of water-soluble heavy crude oil organic-acids, bases, and neutrals by electrospray ionization and field desorption ionization Fourier transform ion cyclotron resonance mass spectrometry. Envion Sci Technol 2007;41:2696.
[31] Lu PY, Metcalf RL, Carlson EM. Environmental fate of five radiolabeled coal conversion by-products evaluated in a laboratory model ecosystem. Environ Health Perspect 1978;24:201.
[32] Hughey CA, Hendrickson CL, Rodgers RP, Marshall AG. Elemental composition analysis of processed and unprocessed diesel fuel by electrospray ionization Fourier transform ion cyclotron resonance mass spectrometry. Energy Fuels 2001;15:1186.
[33] Hughey CA, Rodgers RP, Marshall AG, Qian K, Robbins WK. Identification of acidic NSO compounds in crude oils of different geochemical origins by negative ion electrospray Fourier transform ion cyclotron resonance mass spectrometry. Org Geochem 2002;33:743.
[34] Bellou S, Aggelis G. Biochemical activities in *Chlorella sp*. and *Nannochloropsis salina* during lipid and sugar synthesis in a lab-scale open pond simulating reactor. J Biotechnol 2012;164:318.
[35] Chiavari G, Galletti GC. Pyrolysis–gas chromatography/mass spectrometry of amino acids. J Anal Appl Pyrol 1992;24:123.
[36] Ferreira MMC. Polycyclic aromatic hydrocarbons: a QSPR study chemosphere 2001;44:125.
[37] Yaylayan VA, Kaminsky E. Isolation and structural analysis of Maillard polymers: caramel and melanoidin formation in glycine/glucose model system. Food Chem 1998;63:25.
[38] Simoneit BRT, Rushdi AI, Abas MRB, Didyk BM. Alkyl amides and nitriles as novel tracers for biomass burning. Environ Sci Technol 2003;37:16.
[39] Jena U, Das KC, Kastner JR. Effect of operating conditions of thermochemical liquefaction on biocrude production from *Spirulina platensis*. Bioresour Technol 2011;102:6221.
[40] Ross AB, Biller P, Kubacki ML, Li H, Lea-Langton A, Jones JM. Hydrothermal processing of microalgae using alkali and organic acids. Fuel 2010;89:2234.
[41] Biller P, Riley R, Ross AB. Catalytic hydrothermal processing of microalgae: decomposition and upgrading of lipids. Bioresour Technol 2011;102:4841.
[42] Herod AA, Bartle KD, Kandiyoti R. Characterization of heavy hydrocarbons by chromatographic and mass spectrometric methods: an overview. Energy Fuels 2007;21:2176.
[43] Duan P, Savage PE. Catalytic hydrotreatment of crude algal bio-oil in supercritical water. Appl Catal B 2011;104:136.
[44] Zhou D, Zhang L, Zhang S, Fu H, Chen J. Hydrothermal liquefaction of macroalgae enteromorpha prolifera to bio-oil. Energy Fuels 2010;24:4054.
[45] Zou S, Wu Y, Yang M, Li C, Tong J. Thermochemical catalytic liquefaction of the marine microalgae dunaliella tertiolecta and characterization of bio-oils. Energy Fuels 2009;23:3753.
[46] Garcia-Perez M, Chaala A, Pakdel H, Kretschmer D, Roy C. Characterization of bio-oils in chemical families. Biomass Bioenergy 2007;31:222.
[47] Slavcheva E, Shone B, Turnbull A. Review of naphthenic acid corrosion in oil refining. Br Corros J 1999;34:125.
[48] Holmes SA, Thompson LF. Nitrogen compound distributions in hydrotreated shale oil products from commercial-scale refining. Fuel 1983;62:709.
[49] Klein GC, Rodgers RP, Marshall AG. Identification of hydrotreatment-resistant heteroatomic species in a crude oil distillation cut by electrospray ionization FT-ICR mass spectrometry. Fuel 2006;85:2071.

[50] Wildschut J, Melián-Cabrera I, Heeres HJ. Catalyst studies on the hydrotreatment of fast pyrolysis oil. Appl Catal B 2010;99:298.
[51] Fu J, Klein GC, Smith DF, Kim S, Rodgers RP, Hendrickson CL, et al. Comprehensive compositional analysis of hydrotreated and untreated nitrogen-concentrated fractions from syncrude oil by electron ionization, field desorption ionization, and electrospray ionization ultrahigh-resolution FT-ICR mass spectrometry. Energy Fuels 2006;20:1235.
[52] Zhang T, Zhang L, Zhou Y, Wei Q, Chung KH, Zhao S, et al. Transformation of nitrogen compounds in deasphalted oil hydrotreating: characterized by electrospray ionization Fourier transform-ion cyclotron resonance mass spectrometry. Energy Fuels 2013;27:2952.
[53] Bandu ML, Watkins KR, Bretthauer ML, Moore CA, Desaire H. Prediction of MS/MS Data. 1. A focus on pharmaceuticals containing carboxylic acids. Anal Chem 2004;76:1746.
[54] Grossert JS, Fancy PD, WR L. Fragmentation pathways of negative ions produced by electrospray ionization of acyclic dicarboxylic acids and derivatives. Can J Chem 2005;83:1878.